

## Magnetic coupling in ferromagnetic semiconductor (Ga,Mn)As/(Al,Ga,Mn)As bilayers

M. Wang<sup>1</sup>, P. Wadley, R. P. Campion, A. W. Rushforth, K. W. Edmonds, B. L. Gallagher, T. R. Charlton, C. J. Kinane, and S. Langridge

Citation: *Journal of Applied Physics* **118**, 053913 (2015); doi: 10.1063/1.4928206

View online: <http://dx.doi.org/10.1063/1.4928206>

View Table of Contents: <http://aip.scitation.org/toc/jap/118/5>

Published by the *American Institute of Physics*

---

---



Small Conferences. BIG Ideas.

Applied Physics  
Reviews

**SAVE THE DATE!**  
**3D Bioprinting: Physical and Chemical Processes**  
May 2–3, 2017 • Winston Salem, NC, USA

The background of the banner features a stylized, glowing blue and red network of lines, resembling a biological or chemical structure, set against a dark blue background.

## Magnetic coupling in ferromagnetic semiconductor (Ga,Mn)As/(Al,Ga,Mn)As bilayers

M. Wang,<sup>1,a)</sup> P. Wadley,<sup>1</sup> R. P. Campion,<sup>1</sup> A. W. Rushforth,<sup>1</sup> K. W. Edmonds,<sup>1</sup>  
 B. L. Gallagher,<sup>1</sup> T. R. Charlton,<sup>2</sup> C. J. Kinane,<sup>2</sup> and S. Langridge<sup>2</sup>

<sup>1</sup>*School of Physics and Astronomy, University of Nottingham, University Park, Nottingham NG7 2RD, United Kingdom*

<sup>2</sup>*ISIS, Rutherford Appleton Laboratory, Harwell Science and Innovation Campus, Science and Technology Facilities Council, Oxon OX11 0QX, United Kingdom*

(Received 16 April 2015; accepted 28 July 2015; published online 6 August 2015)

We report on a study of ferromagnetic semiconductor (Ga,Mn)As/(Al,Ga,Mn)As bilayers using magnetometry and polarized neutron reflectivity (PNR). From depth-resolved characterization of the magnetic structure obtained by PNR, we concluded that the (Ga,Mn)As and (Al,Ga,Mn)As layers have in-plane and perpendicular-to-plane magnetic easy axes, respectively, with weak inter-layer coupling. Therefore, the layer magnetizations align perpendicular to each other under low magnetic fields and parallel at high fields. © 2015 AIP Publishing LLC.

[<http://dx.doi.org/10.1063/1.4928206>]

The interfacial coupling between ferromagnetic films has been widely studied, both for fundamental interest and for its relevance to magnetic sensing technologies. In metallic multilayers, direct exchange coupling between neighboring magnetic layers can be avoided by inserting non-magnetic spacers. The resulting interlayer exchange coupling mediated across the spacer can favor parallel, antiparallel, or non-collinear alignment of the magnetic layers, depending on the layer thicknesses and composition.<sup>1</sup>

Interlayer exchange coupling has also been investigated in dilute magnetic semiconductor (DMS) systems. (Ga,Mn)As is a well-studied DMS which exhibits ferromagnetic behavior due to a coupling of the local magnetic moments via delocalized charge carriers, both provided by the substitutional Mn.<sup>2,3</sup> The highest Curie temperature ( $T_C$ ) of this material is around 190 K.<sup>4-6</sup> The magnetic properties of (Ga,Mn)As-based multilayers are highly tunable through manipulation of parameters such as the Mn concentration, epitaxial strain, and doping. For example, while the interlayer exchange coupling is usually ferromagnetic in (Ga,Mn)As/GaAs/(Ga,Mn)As structures,<sup>7,8</sup> antiferromagnetic alignment can be realized by *p*-type doping of the GaAs spacer.<sup>9</sup> Elsewhere, the coupling between compressive-strained (Ga,Mn)As and tensile-strained (Ga,Mn)(As,P) has been utilized in demonstrations of electric-field controlled magnetic anisotropy.<sup>10</sup>

In the quaternary DMS material (Al,Ga,Mn)As, increasing the Al composition results in a reduction of the  $T_C$  and in the electrical conductivity.<sup>11,12</sup> When the conductivity of the material goes from metallic to insulating, the magnetic easy axis undergoes a transition from in-plane to out-of-plane. We recently investigated the growth and properties of (Ga,Mn)As/(Al,Ga,Mn)As bilayer films, with a specific focus on the effect of low-temperature annealing.<sup>13</sup> It was shown that the out-diffusion of interstitial Mn depends on the quality of the

interface between the two materials. Interstitial Mn is a well-known compensating defect in (Ga,Mn)As and (Al,Ga,Mn)As which inhibits the magnetic order.<sup>14-17</sup> For an interface roughness larger than around 0.4 nm, Mn interstitials out-diffuse from the top (Ga,Mn)As layer to the surface, but are inhibited from escaping from the buried (Al,Ga,Mn)As layer, resulting in a large difference in the magnetic properties of the two layers.<sup>13</sup>

In this paper, we focus on the layer-resolved magnetic order in a bilayer (Ga,Mn)As/(Al,Ga,Mn)As film. While conventional magnetometry yields only average magnetization values, integrated over the entire volume of the specimen, polarized neutron reflectometry (PNR) provides a way to determine both the structural and magnetic profile in nanoscale systems.<sup>18</sup> As the neutron scattering cross-section is sensitive to components of the magnetic induction orthogonal to the neutron's momentum transfer, the probe measures the in-plane components of the magnetization. Any rotation from an in-plane to out-of-plane moment will result in an effective reduction of the observed cross-section.

The bilayer sample, consisting of 20 nm of (Al<sub>0.30</sub>Ga<sub>0.66</sub>Mn<sub>0.04</sub>)As and 7 nm of (Ga<sub>0.94</sub>Mn<sub>0.06</sub>)As, has been grown on a GaAs(001) substrate by molecular beam epitaxy (MBE). For the transition from (Al,Ga,Mn)As to (Ga,Mn)As growth, the As flux was accordingly lowered in order to maintain III/V stoichiometry. Due to the delayed response of the As source, the As flux needed to be reduced before the Al flux was shuttered off, while the Ga and Mn fluxes were kept constant.<sup>13</sup> This resulted in a ~1 nm As deficient layer at the (Ga,Mn)As/(Al,Ga,Mn)As interface, as estimated from the growth rate multiplied by the time between reducing the As flux and shuttering off the Al. The sample was annealed in air at 180 °C in order to induce ferromagnetic order in the buried (Al,Ga,Mn)As layer. Annealing results in a diffusion of Mn interstitial defects to the surface where they oxidize, producing in a Mn-rich surface oxide layer.<sup>15</sup> X-ray reflectivity (XRR) was performed using an X'Pert materials

<sup>a)</sup>Current address: London Centre for Nanotechnology, University College London, 17-19 Gordon Street, London WC1H 0AH, United Kingdom.

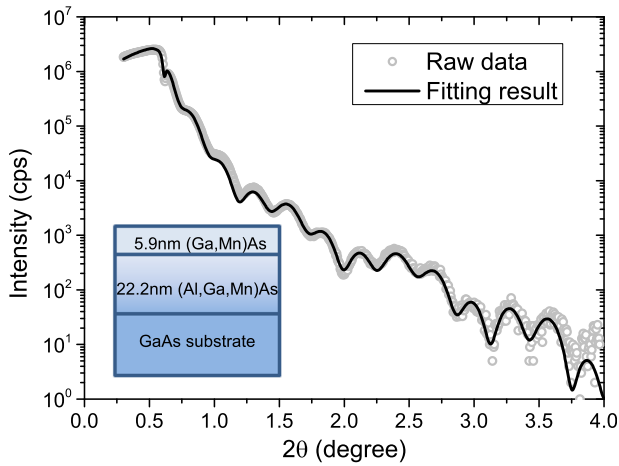


FIG. 1. X-ray reflectivity measurement of the partial annealed sample and the resultant fit. The inset depicts the sample structure obtained from the fit. The 3 nm oxidized surface layer has not been shown in this schematic.

research diffractometer system, in order to investigate the layer structure of the sample (Fig. 1). Fitting by using the PANalytical X'Pert Reflectivity software yielded a layer structure consisting of  $22.2 \pm 0.2$  nm  $(\text{Al}_{0.30}\text{Ga}_{0.66}\text{Mn}_{0.04})\text{As}$  layer with a  $1.1 \pm 0.1$  nm As-deficient interface region,  $5.9 \pm 0.1$  nm  $(\text{Ga}_{0.94}\text{Mn}_{0.06})\text{As}$  layer and a  $3.0 \pm 0.2$  nm oxidized surface.

We characterized the magnetic properties of the as-grown, 7.5 h partial annealed and 48 h fully annealed sample using a Quantum Design superconducting quantum interference device (SQUID) magnetometer. The remnant magnetization along different crystal directions, measured versus increasing temperature after cooling to 2 K in a 1000 Oe magnetic field, are shown in Figs. 2(a) and 2(b). In the as-grown state, projections of the remnant magnetic moment are observed along the orthogonal in-plane  $[110]$  and  $[\bar{1}\bar{1}0]$  directions and the out-of-plane  $[001]$  direction at the lowest temperature. On increasing the temperature, the  $[001]$ ,  $[110]$ , and  $[\bar{1}\bar{1}0]$  projected remnant moments disappear at around 4 K, 19 K, and 36 K, respectively. The 4 K transition is ascribed to the  $T_C$  of the  $(\text{Al,Ga,Mn})\text{As}$  layer, with perpendicular magnetic anisotropy. The decay of the  $[110]$  projected moment at 19 K is ascribed to a spin reorientation transition in the  $(\text{Ga,Mn})\text{As}$ , with a dominant biaxial magnetic anisotropy favoring  $[100]/[010]$  easy axes at low temperatures, making way to a uniaxial anisotropy favoring the  $[\bar{1}\bar{1}0]$  orientation at higher temperatures. This behavior is commonly observed in  $(\text{Ga,Mn})\text{As}$  under compressive strain.<sup>19</sup> Finally, the disappearance of the  $[\bar{1}\bar{1}0]$  projected moment at 36 K is ascribed to the  $T_C$  of the  $(\text{Ga,Mn})\text{As}$  layer.

After 7.5 h annealing, the  $[001]$  projected moment is increased by more than a factor of two compared to its

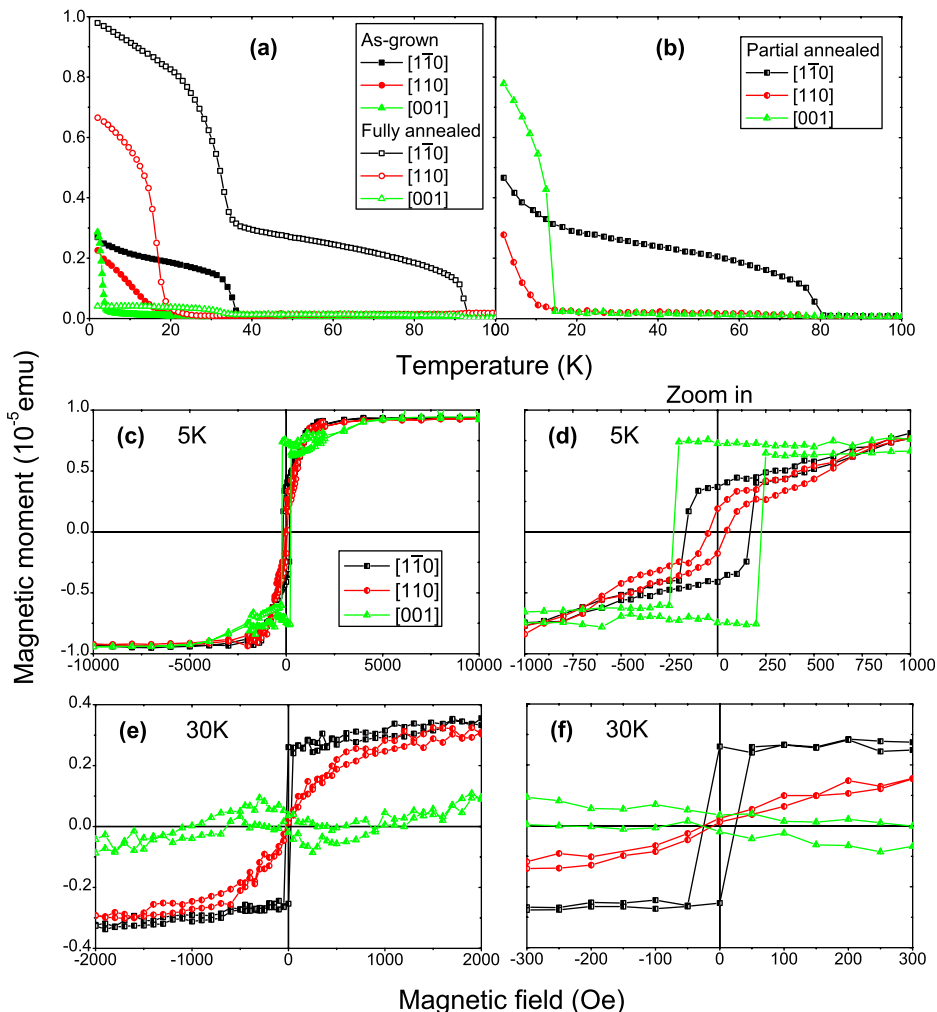


FIG. 2. Projection of thermo-remnant magnetization along  $[\bar{1}\bar{1}0]$ ,  $[110]$ , and  $[001]$  directions of (a) as-grown and fully annealed, (b) partially annealed sample, and (c)–(f) the hysteresis loops along  $[\bar{1}\bar{1}0]$ ,  $[110]$ , and  $[001]$  directions of the partially annealed sample measured at 5 K and 30 K.

as-grown value, and it persists to around 14 K. The  $T_C$  of the (Ga,Mn)As layer, inferred from the disappearance of the  $[1\bar{1}0]$  projected moment, is around 81 K. After 48 h annealing, the projected remnant moment along the  $[001]$  orientation is very small, indicating that both the (Ga,Mn)As and the (Al,Ga,Mn)As layers now have in-plane magnetic anisotropy. The  $T_C$  of the (Ga,Mn)As in this fully annealed state is around 93 K, while for the (Al,Ga,Mn)As a  $T_C$  of 35 K is estimated from the sharp decay of the  $[1\bar{1}0]$  projected remnant moment around this temperature. Hysteresis loops for the annealed sample at 5 K and 30 K are shown in Figs. 2(c) and 2(d) and Figs. 2(e) and 2(f), respectively.

The PNR measurement was carried out on the Polref reflectometer<sup>20</sup> at the ISIS pulsed neutron and muon source, Rutherford Appleton Laboratory. The 7.5 h partial annealed sample was measured with in-plane projection of the incident beam along the  $[110]$  crystalline axis, and magnetic field along  $[1\bar{1}0]$ . The sample was first field cooled from room temperature to 5 K under 9000 Oe magnetic field, which is high enough to saturate the magnetization for both layers in the  $[1\bar{1}0]$  direction (see Fig. 2(c)). Then, the neutron specular reflectivities were measured for neutron spin eigenstates parallel ( $R^+$ ) and antiparallel ( $R^-$ ) to the magnetic field direction. Measurements were performed under magnetic fields of <60 Oe and 9000 Oe, at sample temperatures of 5 K and 30 K.

Fig. 3 shows the measured neutron reflectivities normalized to the Fresnel reflectivity of the GaAs substrate. The PNR data were modelled using the Refl1D<sup>21</sup> specular reflectometry modelling and fitting software. The fitting parameters are the layer thicknesses, interface roughness, real ( $\rho$ ) component of the nuclear scattering length density (SLD), and the magnetic SLD ( $\rho_M$ ).<sup>18</sup> Because the oxidized surface and GaAs substrate should be non-ferromagnetic, the  $\rho_M$  for these layers has been fixed to zero. The structural properties of the materials (layer thickness, interface roughness and  $\rho$ ,

which is proportional to the density of the material), are magnetic field and temperature independent. The values of these parameters should be consistent with the XRR fitting results. Therefore, these parameters were initialized with the values obtained from the XRR before fitting the PNR data sets without constraint.

Table I presents the fitting results of the PNR data. The layer thickness, interface roughness, and density for each layer are consistent in different temperatures and magnetic fields scenarios. The results show that there is a  $5.3 \pm 0.2$  nm (Ga,Mn)As layer on top of the  $22.8 \pm 0.2$  nm (Al,Ga,Mn)As layer with interface roughness around 0.4 nm. The interface roughness between the bottom layer and the substrate is very close to zero. The density for each layer has been obtained from the nuclear SLD, and the magnetic SLDs have been converted to magnetizations for the (Ga,Mn)As and (Al,Ga,Mn)As layers, assuming  $1 \times 10^{-6} \text{ \AA}^{-2} = 340 \text{ emu per cubic centimeter}$ .<sup>17</sup>

Fig. 4 shows the depth profiles of  $\rho_M$  and  $\rho$  extrapolated from PNR fits. The fitted values for  $\rho$  are within 10% of the XRR results (Table I). The values of  $\rho_M$  reflect the thickness-dependence of the magnetic structure across the sample. For the 5 K 9000 Oe scenario, both layers have large  $\rho_M$ , indicating that the magnetization is saturated along the in-plane  $[1\bar{1}0]$  direction of the applied magnetic field. When the magnetic field is reduced to below 60 Oe, the  $\rho_M$  of the bottom (Al,Ga,Mn)As layer is decreased by around 84%, suggesting that the magnetic moments in this layer are aligned nearly parallel to the  $[001]$  direction. In addition, the  $\rho_M$  of the top layer is reduced by about 23% which may be due to canting of the layer magnetization towards the  $[001]$  due to exchange coupling with the lower layer. Combining this with the results from SQUID measurements (Fig. 2), we can conclude that at 5 K the magnetization of the (Al,Ga,Mn)As layer is roughly out-of-plane, perpendicular to the magnetization orientation of the (Ga,Mn)As layer. The reduction in the  $\rho_M$  for the two

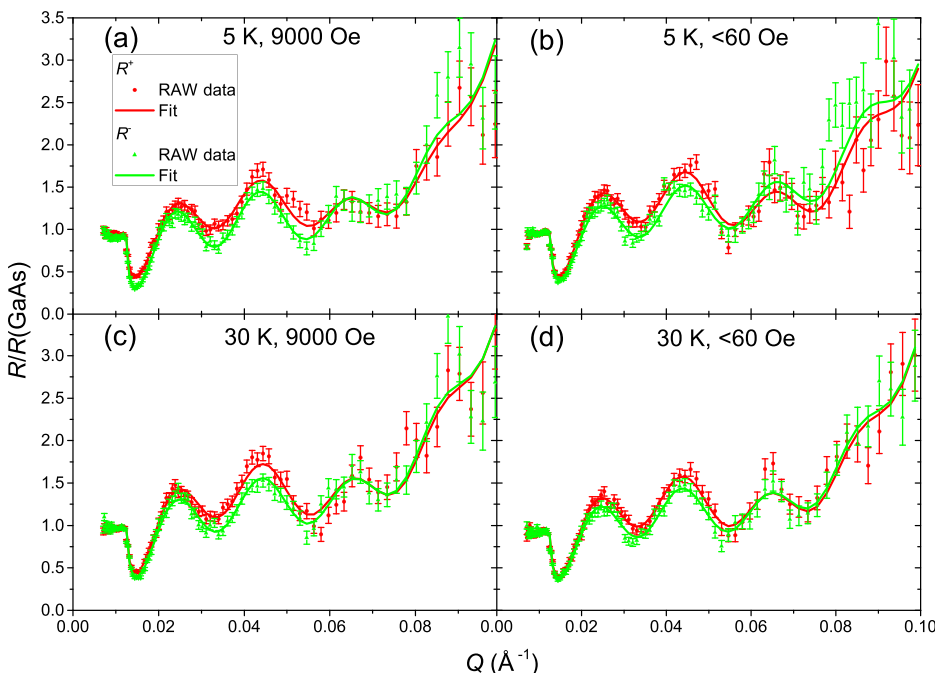


FIG. 3. The measured results and fits of the Fresnel normalized polarized neutron reflectivities for varying field and temperature conditions.

TABLE I. The polarized neutron reflectivity and x-ray reflectivity fitting results.

Layer	Parameters	PNR				XRR
		5 K		30 K		
		9000 Oe	60 Oe	9000 Oe	60 Oe	
Oxidized surface	Roughness (nm)	$0.6 \pm 0.1$	$0.7 \pm 0.1$	$0.6 \pm 0.2$	$0.7 \pm 0.1$	$0.7 \pm 0.1$
	$\rho$ ( $10^{-6} \text{ \AA}^{-2}$ )	$2.8 \pm 0.1$	$3.1 \pm 0.1$	$3.0 \pm 0.1$	$3.0 \pm 0.1$	
	$\rho$ ( $\text{g cm}^{-3}$ )	$4.3 \pm 0.2$	$4.8 \pm 0.2$	$4.6 \pm 0.2$	$4.6 \pm 0.2$	$4.6 \pm 0.2$
	Thickness (nm)	$2.4 \pm 0.1$	$2.6 \pm 0.1$	$2.3 \pm 0.1$	$2.4 \pm 0.1$	$3.0 \pm 0.2$
GaMnAs	Roughness (nm)	$0.5 \pm 0.1$	$0.5 \pm 0.1$	$0.4 \pm 0.1$	$0.4 \pm 0.1$	$0.4 (<0.7)$
	$\rho_M$ ( $10^{-6} \text{ \AA}^{-2}$ )	$0.120 \pm 0.005$	$0.093 \pm 0.005$	$0.084 \pm 0.005$	$0.067 \pm 0.005$	
	$M$ ( $10^{-5} \text{ emu cm}^{-3}$ )	$41 \pm 2$	$32 \pm 2$	$28 \pm 2$	$23 \pm 2$	
	$\rho$ ( $10^{-6} \text{ \AA}^{-2}$ )	$3.3 \pm 0.1$	$3.4 \pm 0.1$	$3.3 \pm 0.1$	$3.3 \pm 0.1$	
	$\rho$ ( $\text{g cm}^{-3}$ )	$5.7 \pm 0.2$	$5.8 \pm 0.2$	$5.8 \pm 0.2$	$5.6 \pm 0.2$	$5.6 \pm 0.2$
	Thickness (nm)	$5.2 \pm 0.2$	$5.5 \pm 0.2$	$5.4 \pm 0.2$	$5.3 \pm 0.2$	$5.9 \pm 0.1$
AlGaMnAs	Roughness (nm)	$0.4 \pm 0.1$	$0.6 \pm 0.1$	$0.5 \pm 0.1$	$0.4 \pm 0.1$	$0.3 (<0.5)$
	$\rho_M$ ( $10^{-6} \text{ \AA}^{-2}$ )	$0.050 \pm 0.002$	$0.008 \pm 0.001$	$0.014 \pm 0.001$	$0.004 \pm 0.001$	
	$M$ ( $10^{-5} \text{ emu cm}^{-3}$ )	$17.1 \pm 0.7$	$2.8 \pm 0.4$	$4.7 \pm 0.4$	$1.5 \pm 0.4$	
	$\rho$ ( $10^{-6} \text{ \AA}^{-2}$ )	$2.7 \pm 0.1$	$2.8 \pm 0.1$	$2.8 \pm 0.1$	$2.8 \pm 0.1$	
	$\rho$ ( $\text{g cm}^{-3}$ )	$4.9 \pm 0.2$	$5.0 \pm 0.2$	$5.0 \pm 0.2$	$4.9 \pm 0.2$	$4.8 \pm 0.2$
	Thickness (nm)	$23.0 \pm 0.2$	$22.7 \pm 0.1$	$22.6 \pm 0.1$	$22.8 \pm 0.2$	$22.2 \pm 0.2$
GaAs	Roughness (nm)	$\sim 0$	$\sim 0$	$\sim 0$	$\sim 0$	$\sim 0$
	$\rho$ ( $10^{-6} \text{ \AA}^{-2}$ )	$3.2 \pm 0.1$	$3.2 \pm 0.1$	$3.2 \pm 0.1$	$3.2 \pm 0.1$	
	$\rho$ ( $\text{g cm}^{-3}$ )	$5.5 \pm 0.1$	$5.6 \pm 0.1$	$5.6 \pm 0.2$	$5.6 \pm 0.2$	$5.3 \pm 0.2$
	$\chi^2$	22.18	30.73	15.51	24.07	

layers on reducing the field is consistent with the reduction in the total moment seen in Figs. 2(c) and 2(d). According to the depth profile of the extrapolated magnetic SLD, the magnetization changes sharply over a distance of  $1.6 \pm 0.3$  nm across the (Al,Ga,Mn)As/(Ga,Mn)As interface region.

At 30 K,  $\rho_M$  for the (Al,Ga,Mn)As layer is close to zero when the magnetic field is below 60 Oe, and it increases to around  $1.4 \times 10^{-8} \text{ \AA}^{-2}$  under a 9000 Oe applied field. Consistent with the absence of a remanent magnetization at

30 K after field-cooling along the out-of-plane [001] orientation (Fig. 2(b)), this indicates that the (Al,Ga,Mn)As layer is paramagnetic at this temperature. For the (Ga,Mn)As layer,  $\rho_M$  reduced by 20% as field decreases from 9000 Oe to  $<60$  Oe, similar to the behavior observed at 5 K. The orientation of magnetization for individual layers of the sample in different scenarios is shown in the insets of Fig. 4.

In summary, we have investigated the structure and magnetic properties of the (Ga,Mn)As/(Al,Ga,Mn)As bilayer thin

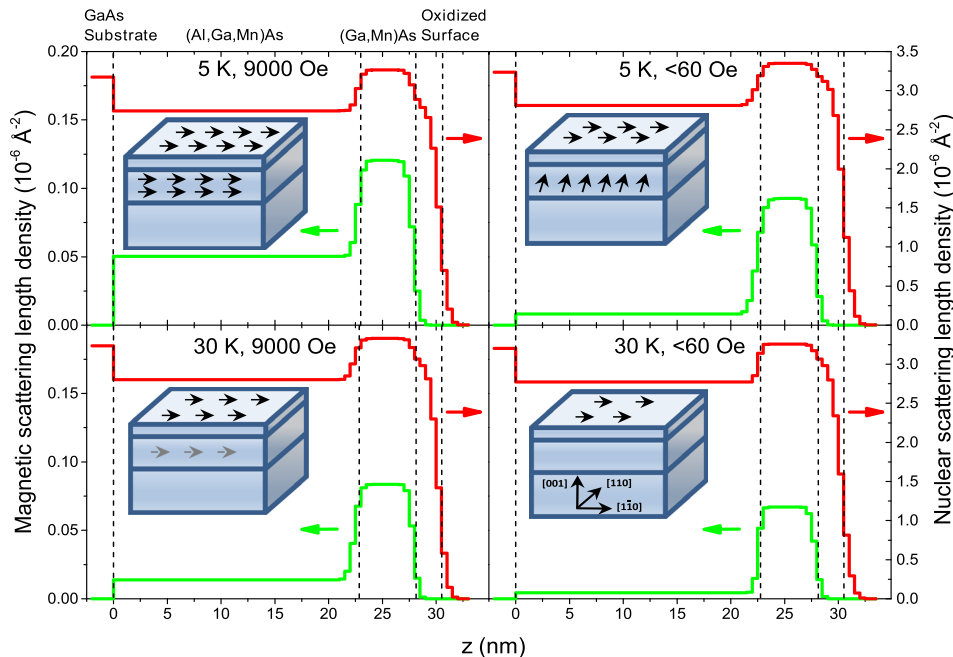


FIG. 4. Magnetic and nuclear scattering length density depth profiles extrapolated from the fits of polarized neutron reflectivities. The insets show the magnetization for each layer in different scenarios.

film materials. Using the PNR technique, we obtained the quantitative magnetic properties for each layer at different temperatures and magnetic fields. The PNR results are consistent with data from the conventional magnetometry method, but crucially, provide a self-calibrating depth resolution. Our results show that instead of an antiferromagnetic coupling between the two layers, their magnetizations are nearly perpendicular to one another at 5 K when the applied field was close to zero, and parallel to one another at higher field values. The sharp transition from out-of-plane to in-plane is indicative of weak interlayer coupling. The unique and controllable interlayer magnetic arrangement indicated in our results suggests that this material structure can be a good candidate for memory device applications.

We acknowledge ISIS pulsed neutron and muon source at the Rutherford Appleton Laboratory for the provision of beamtime, and funding from EU grant FP7-214499—NAMASTE, EU ERC advanced grant 268066, and EPSRC grant EP/H002294.

<sup>1</sup>B. Heinrich, *Springer Tracts Mod. Phys.* **227**, 185 (2008).

<sup>2</sup>T. Dietl and H. Ohno, *Rev. Mod. Phys.* **86**, 187 (2014).

<sup>3</sup>T. Jungwirth, J. Wunderlich, V. Novak, K. Olejnik, B. L. Gallagher, R. P. Campion, K. W. Edmonds, A. W. Rushforth, A. J. Ferguson, and P. Nemeč, *Rev. Mod. Phys.* **86**, 855 (2014).

<sup>4</sup>M. Wang, R. P. Campion, A. W. Rushforth, K. W. Edmonds, C. T. Foxon, and B. L. Gallagher, *Appl. Phys. Lett.* **93**, 132103 (2008).

<sup>5</sup>V. Novak, K. Olejnik, J. Wunderlich, M. Cukr, K. Vyborny, A. W. Rushforth, K. W. Edmonds, R. P. Campion, B. L. Gallagher, J. Sinova, and T. Jungwirth, *Phys. Rev. Lett.* **101**, 077201 (2008).

<sup>6</sup>M. Wang, K. W. Edmonds, B. L. Gallagher, A. W. Rushforth, O. Makarovskiy, A. Patane, R. P. Campion, C. T. Foxon, V. Novak, and T. Jungwirth, *Phys. Rev. B* **87**, 121301 (2013).

<sup>7</sup>H. Kępa, J. Kutner-Pielaszek, A. Twardowski, C. F. Majkrzak, J. Sadowski, T. Story, and T. M. Giebultowicz, *Phys. Rev. B* **64**, 121302 (2001).

<sup>8</sup>B. J. Kirby, J. A. Borchers, X. Liu, Z. Ge, Y. J. Cho, M. Dobrowolska, and J. K. Furdyna, *Phys. Rev. B* **76**, 205316 (2007).

<sup>9</sup>J. H. Chung, S. J. Chung, S. Lee, B. J. Kirby, J. A. Borchers, Y. J. Cho, X. Liu, and J. K. Furdyna, *Phys. Rev. Lett.* **101**, 237202 (2008).

<sup>10</sup>T. Niazi, M. Cormier, D. Lucot, L. Largeau, V. Jeudy, J. Cibert, and A. Lemaitre, *Appl. Phys. Lett.* **102**, 122403 (2013).

<sup>11</sup>K. Takamura, F. Matsukura, D. Chiba, and H. Ohno, *Appl. Phys. Lett.* **81**, 2590 (2002).

<sup>12</sup>A. W. Rushforth, N. R. S. Farley, R. P. Campion, K. W. Edmonds, C. R. Staddon, C. T. Foxon, B. L. Gallagher, and K. M. Yu, *Phys. Rev. B* **78**, 085209 (2008).

<sup>13</sup>M. Wang, A. W. Rushforth, A. T. Hindmarch, R. P. Campion, K. W. Edmonds, C. R. Staddon, C. T. Foxon, and B. L. Gallagher, *Appl. Phys. Lett.* **102**, 112404 (2013).

<sup>14</sup>K. M. Yu, W. Walukiewicz, T. Wojtowicz, I. Kuryliszyn, X. Liu, Y. Sasaki, and J. K. Furdyna, *Phys. Rev. B* **65**, 201303 (2002).

<sup>15</sup>K. W. Edmonds, P. Boguslawski, K. Y. Wang, R. P. Campion, S. V. Novikov, N. R. S. Farley, B. L. Gallagher, C. T. Foxon, M. Sawicki, T. Dietl, M. B. Nardelli, and J. Bernholc, *Phys. Rev. Lett.* **92**, 037201 (2004).

<sup>16</sup>B. J. Kirby, J. A. Borchers, J. J. Rhyne, S. G. E. te Velthuis, A. Hoffmann, K. V. O'Donovan, T. Wojtowicz, X. Liu, W. L. Lim, and J. K. Furdyna, *Phys. Rev. B* **69**, 081307 (2004).

<sup>17</sup>B. J. Kirby, J. A. Borchers, J. J. Rhyne, K. V. O'Donovan, S. G. E. te Velthuis, S. Roy, C. Sanchez-Hanke, T. Wojtowicz, X. Liu, L. Lim, M. Dobrowolska, and J. K. Furdyna, *Phys. Rev. B* **74**, 245304 (2006).

<sup>18</sup>S. J. Blundell and J. A. C. Bland, *Phys. Rev. B* **46**, 3391 (1992).

<sup>19</sup>K. Y. Wang, M. Sawicki, K. W. Edmonds, R. P. Campion, S. Maat, C. T. Foxon, B. L. Gallagher, and T. Dietl, *Phys. Rev. Lett.* **95**, 217204 (2005).

<sup>20</sup>J. Webster, S. Langridge, R. Dalgliesh, and T. Charlton, *Eur. Phys. J. Plus* **126**, 112 (2011).

<sup>21</sup>P. A. Kienle, J. Krycka, N. Patel, and I. Sahin, REFL1D (Version 0.6.19) [Computer Software], College Park, MD, 2011.